Article:

Carey, J.M., Crutchley, G.J., Mountjoy, J.J. et al. (3 more authors) (2019) Slow episodic movement driven by elevated pore-fluid pressures in shallow subaqueous slopes. Geomorphology, 329. pp. 99-107. ISSN 0169-555X

https://doi.org/10.1016/j.geomorph.2018.12.034

Slow episodic movement driven by elevated pore-fluid pressures in shallow subaqueous slopes

J.M. Carey[1], G.J. Crutchley[1], J.J. Mountjoy[2], D.N. Petley[3] M.J. McSaveney[1] & B. Lyndsell[1]

[1]GNS Science, 1 Fairway Drive Avalon, PO Box 30368 Lower Hutt, New Zealand

[2]National Institute of Water and Atmospheric Research, PO Box 14901, Wellington, New Zealand

[3]Department of Geography, University of Sheffield, Sheffield, S10 2TN, UK

ABSTRACT

Subaqueous slopes are susceptible to a broad range of failure mechanisms and deformation styles, many of which are not well characterised. We undertook novel laboratory-based testing using a Dynamic Back-Pressured Shearbox on samples collected from an area subject to ongoing slope failures, situated on the upper slope of New Zealand's Hikurangi Margin, to determine how increases in pore water and gas pressures generate shallow mass movement. Using both water and nitrogen gas we observed similar responses in both cases, indicating that behaviour is dominated by the normal effective stress state regardless of pore-fluid phase. Shear-strain accumulation, representing landslide movement, shows a slow episodic pattern, in common with many shallow terrestrial landslides. Our results are relevant for landslides occurring in shallow near surface sedimentary sequences but have implications for deep seated landslide behaviour. They suggest that once movement initiates at a critical effective stress, its rate is regulated through dilation and pore expansion within the shear zone, temporarily increasing effective stress within a narrow shear band and supressing rapid shear. Consequently, under certain conditions, shallow submarine landslides (e.g. spreading failures) can undergo slow episodic movement which allows them to accumulate large shear strains without accelerating to catastrophic movement even when they are unconstrained.

1. INTRODUCTION

Although subaqueous mass movements can develop on very gentle slopes (<<2°), they can run out for extremely long distances across the deep ocean floor (Talling et al., 2007). In most cases the slope failures leave an empty scar in the source region with almost all residual strength material evacuated (Krastel et al., 2018; Mountjoy and Micallef, 2018). As source area slopes are predominantly lower than the friction angles of the landslide materials (e.g. Urlaub et al., 2015), the generation of pore pressures exceeding hydrostatic pressure are a likely loading mechanism. But, in some instances, the debris from subaqueous slope failures only moves a short distance before coming to rest despite a lack of buttressing or obvious decrease in slope gradient (Locat and Lee, 2000; Micallef et al., 2013). Such small-displacement mass failures have been found in a wide range of seafloor environments including passive margins (Baeten et al., 2014) and active margins (Micallef et al., 2016). These indicate that there are likely to be common mechanisms for the movement and arrest over a short distance of certain seafloor failures.

The high pore pressures that often initiate movement can occur from widely recognised processes including undrained cyclic loading during earthquakes (e.g. Sassa et al., 2012), rapid sediment burial (e.g. Stigall and Dugan, 2010) and as result of focused fluid flow (e.g. Dugan and Flemings, 2000; Elger et al., 2018). In addition, high pore pressures may be generated by more complex processes involving for example gas liberation from hydrate dissociation (Riboulot et al., 2013).

Despite the advances in understanding potential causes of submarine landslides, the fundamental processes controlling their movement remain poorly constrained compared with their terrestrial counterparts. Over the last century, terrestrial landslides have been shown to display a wide array of movement behaviour, ranging from slow creep (≤ 1 mm a^{-1}) (e.g. Mansour et al., 2011), through episodic sliding and stick-slip (≈ 1 cm a^{-1}) (e.g. Allison and Brunsden, 1990) to acceleration to catastrophic failure (>> 1 m s^{-1}) (e.g. Kilburn and Petley, 2003). Such complex movements are commonly associated with pore fluid pressure-induced changes, as has been hypothesised for subaqueous landslides.

The availability of high resolution landslide monitoring records onshore has allowed detailed acceleration phases in multiple landslides to be examined in a variety of materials (e.g. Schulz et al., 2009; Massey et al., 2013; Carey et al., 2015). These studies distinguish two distinct styles of movement (Petley et al., 2002). The first movement style is brittle, characterised by a distinct hyperbolic acceleration in displacement rate to failure. These movement patterns can be examined by plotting in 1/v – t space (where v is velocity) and yield a negative linear trend to failure which generally results in rapid accelerations and catastrophic landsliding (e.g. Voight, 1988; Fukuzono, 1990; Petley and Petley, 2006). Conversely, the second style of movement is ductile, characterised by an exponential acceleration to a constant strain rate which when analysed in 1/v – t space produces a distinct asymptotic trend (Petley et al., 2005b).

Specialist laboratory testing approaches have been used to simulate landslide failure conditions by increasing pore water pressures at constant normal and shear stress (e.g. Brand, 1981; Anderson and Sitar, 1995; Zhu and Anderson, 1998; Dai et al., 1999; Orense et al., 2004; Petley et al., 2005a, Ng and Petley, 2009; Carey and Petley, 2014). These approaches confirm that movement styles are controlled by mechanisms of deformation occurring within shear zones (Petley et al., 2005a; Ng and Petley, 2009; Carey and Petley, 2014). In cases where brittle shear surface development occurs, the hyperbolic acceleration to final failure is observed in the experiments, whilst exponential acceleration occurs in landslides undergoing ductile deformation (Petley et al., 2005a). Numerous conceptual models have been proposed to explain these different strain responses to changes in stress state, ranging from catastrophic failure driven by micro-cracking and rapid shear-surface propagation (e.g. Petley et al., 2005a; Viesca and Rice, 2012) to slower, steady landslide motion in response to shear-zone dilation and subsequent pore-pressure feedback (e.g. Iverson, 2005).

Given increases in pore-water pressure may drive either of movement-arrest or rapid runout behaviour in terrestrial landslides, depending on the material response, similar behaviour should be expected in subaqueous landslides. The mechanisms controlling the transition from steady slow movement to rapid failure observed in specialist laboratory tests may be key to determining the behaviour of a given subaqueous landslide. However, very few small displacement or reactivated subaqueous landslides have been observed and investigated.

Two subaqueous landslides on the northern Hikurangi Margin located off the east cost of New Zealand have geomorphological characteristics that indicate movement-arrest behaviour may be occurring (Mountjoy et al., 2009; Micallef et al., 2016) making them suitable for investigating this behaviour in subaqueous slopes. In this study, we seek to constrain better the potential movement mechanisms in short displacement and reactivated subaqueous landslides by conducting novel laboratory experiments on sediment samples collected from the shallow sedimentary sequence on the northern

Hikurangi Margin area. We use a Dynamic Back-Pressured Shearbox (DBPSB) to accurately replicate in-situ stresses in the submarine slopes to explore the potential strain response of the landslide when subject to elevated pore water and gas pressure.

2. SAMPLE AREA

An area of the upper continental slope on the Hikurangi Subduction Margin, off the coast of Gisborne, New Zealand, hosts a number of landslides where limited displacement has occurred following their initial failure (Mountjoy et al., 2009; Micallef et al., 2016) or where repeated reactivation has been hypothesised (Mountjoy et al., 2014) (Figure 1 A and B). The landslides occur within an active subduction zone experiencing regular tectonic activity (Wallace and Bevan, 2010; Wallace et al., 2012). The upper continental slope is comprised of Miocene to Recent slope basin sequences (Mountjoy et al., 2009). A gravity core profile down the length of the slides (the Tuaheni Landslide Complex) shows that the upper few metres of sediment are dominated by mud to sand sized particles from hemipelagic drape, reworked landslide debris and airfall tephra (Kuhlmann et al., 2018).

The Tuaheni Landslide Complex (TLC) comprises an area of approximately 145 km^2 which is sub-divided into Tuaheni North and Tuaheni South, separated by a 2 km wide spur (Figure 1 A). While Tuaheni North is characterised by multiple evacuated landslide scarps, Tuaheni South is characterised by a large debris apron which has a distinct scarp and bench topography and features indicative of lateral, extensional and compressional deformation (Mountjoy et al., 2009; 2014). The base of gas hydrate stability has been imaged beneath the TLC's extensional domain and it has been suggested that the gas hydrate system may play a role in deformation of the landslide mass (Mountjoy et al., 2014; Crutchley et al., 2016). Although no movement measurements are available, the morphology of Tuaheni South is similar to slow-moving landslide complexes observed in terrestrial environments such as earthflows and mudslides (e.g. Hungr et al., 2014) which occur in similar fine-grained sediments and are often subject to episodic remobilisation (e.g. Alison and Brunsden, 1990). Seismic-reflection surveys across the landslide immediately north of TLC (Figure 1 C) indicate that there is free gas in the proto basal failure surface, and adjacent to the landslide, but gas is not observed beneath the landslide body (Micallef et al., 2016). This suggests that free gas may have been present in the slope prior to the landslides and that the gas migrated out of the sediment sequence during and/or after failure. Micallef et al., (2016) concluded that overpressure in the slope sequence may have contributed to bringing the slope to the point of failure, and that once the landslide moved and dilated, the gas pressure reduced, and further failure was arrested. To further test this interpretation required measurement of relevant geotechnical data, and this provided an opportunity to assess different mechanisms that result in small-displacement slope failures.

3. MATERIALS AND METHODS

We performed a suite of conventional laboratory experiments to determine the physical and geomechanical characteristics of the shallow materials collected from the landslide complex (Tables 1 and 2). Sediment samples were collected from the crest of the landslide (Tan1404-02) and from within an extensional domain farther downslope (Tan1404-10) (Figure 1 A) using a 100 mm diameter gravity corer during RV Tangaroa voyage TAN1404 in April/May 2014.

These standard soil classification test results indicate that both materials have similar physical properties (Table 1). Natural water contents were higher in the shallow EN1285 samples (Tan1404-02) and had correspondingly higher void ratios and lower dry densities when compared with deeper EN1287 samples (Tan1404-10). Particle-size analyses (Figure 2) confirm that both materials are fine grained comprising of over 88 % silt, approximately 5 % clay and with the remaining fraction consisting of mostly fine and medium grained sand. The Atterberg Limit tests performed for both samples confirmed similar plastic and liquid limits and universal soil classifications at the boundary of high plasticity silts and clays (Table 1). The results indicated that the physical properties of the sediments were similar both within the downslope extensional domain and above the current landslide crest, indicating that any sediment disturbance during sampling would have negligible impact on our study.

Conventional drained direct shear tests were undertaken on 60 mm diameter circular samples of both materials using a Wykeham Farrance direct shearbox WF2500. Shearing was conducted at three low normal stresses (Table 2) to simulate the shallow depths of burial of the samples. Shearing was initiated on completion of the consolidation phase (i.e., no further significant vertical displacement at the desired normal load for shearing). A slow shear rate (1.83×10^{-4} mm s^{-1}), was used to avoid developing excess pore pressures within the specimens and a minimum of five shear reversals was completed for each test to ensure a representative ‘residual’ shear strength was reached (i.e., no further reduction in shearing stress on cyclic loading).

A suite of specialist pore-pressure reinflation experiments was performed in the Dynamic Back-Pressured Shearbox (Figure 3), constructed by GDS Instruments Ltd and described in detail by Brain et al. (2015) and Carey et al. (2016). Previous studies have demonstrated that the DBPSB is able to induce a variety of styles of deformation ranging from dynamic liquefaction (Carey et al. 2017) to creep (Carey et al. 2016). Each sample was saturated prior to testing to replicate the shallow seabed conditions (Table 3) using methods previously described (see Carey et al., 2016). A normal effective stress of 32 kPa was applied to each sample during consolidation by applying a back pressure of 100 kPa and a total normal stress at 132 kPa.

After consolidation, each sample was sheared to failure at a constant strain rate (1.83 x 10^{-4} mm s^{-1}, chosen to avoid excess pore fluid generation) to form a shear zone representative of the base of a shallow subaqueous landslide, and to measure initial shear strength. A shear-stress of c.70 % of the undrained strength was then applied to each sample, whereupon both total normal and total shear stress were held constant whilst the normal effective stress was reduced by increasing pore pressure until the samples failed (Figure 4). The experiments were conducted using two different pore fluid conditions: water, and water plus nitrogen gas.

Pore-water pressure controlled tests (referred to as PWP) were conducted by linearly increasing the back pressure applied to the sample whilst holding both the total normal stress and shear stress constant (Figure 3B). De-aired water was used to ensure that the pore-water pressure increases and changes in fluid movement pathways anticipated in the shallow seabed were accurately simulated.

Pore-gas pressure controlled experiments (referred to as PGP) were conducted using nitrogen gas because it has similar physical properties to methane for the conditions of our tests (Kossel et al. 2013), but is safer to use than methane. PGP experiments were performed by filling the volume controller (VC1) with nitrogen gas whilst a second volume controller (VC2) was used to maintain the back pressure to the sample (Figure 3C). VC1 was raised to the same pressure as the vessel before being connected to the sample. Once the pressures were equal, the gas volume controller was opened to the base of the sample and monitored to ensure that no significant pressure change occurred in either volume controller, and that no sample strain occurred prior to the test run. The pressure in the gas volume controller was then increased linearly at rates of 12 kPa/hr and 30 kPa/hr to replicate increasing gas pressure within a shear zone. The porous disc, installed at the sample base was replaced with a specially designed gas test plug prior to testing to ensure gas pressures would be applied to the sample shear zone (Figure 3 C). To ensure that the gas was replacing the water within the soil pores, VC1 was allowed to increase in volume (to extract water) as gas pressure was increased (Figure 3 C). These PGP tests using the DBPSB were the first of their kind, representing a new methodology for testing the impact of gas pressure on sediment failure. Both the PWP and PGP testing approaches resulted in similar stress paths to failure in which increasing pore-fluid pressures resulted in a reduction in mean effective stress toward failure while shear stress and total normal stresses remained constant (Figure 4).

During each phase of pore-fluid pressure increase, shear strain was monitored by measuring the horizontal (shear) displacement of the shear box. These experiments simulated the generation of excess pore-fluid pressure, and associated shear-strain response, in near surface subaqueous landslides under a representative stress state.

4. LABORATORY RESULTS

The conventional shear box tests indicated no notable peak strength or shear strength reduction following repeated shear reversals (Table 2) consistent with ductile behaviour. Shear tests at three confining pressures indicated that the sediments had a linear drained failure envelope, with similar friction angles which ranged between 34° and 36° with an effective cohesion of 4.0 kPa (Figure 5). The strength characteristics measured in the landslide materials were comparable, with similar materials tested from other fine-grained subaqueous landslide systems (e.g. Sassa et al., 2012).

The horizontal (shear) strain and vertical (axial) strain behaviour were found to be broadly consistent in all three PWP tests regardless of rate of pore water pressure increase (Figure 6 A and B). In each experiment horizontal deformation progressed through three movement phases as the shear zone dilated; these three phases can be observed by distinct changes in horizontal strain rate (Figure 7).

An initial low strain rate ($< 0.05\ \mu S\ s^{-1}$) was observed in each sample whilst the mean effective stress (p’) remained high (Figure 7). The strain rate of this early phase of shear-zone deformation increased exponentially in response to the reducing mean effective stress and corresponding sample dilation. This initial phase was followed by a distinct sliding phase which was characterised by a rapid increase and then decrease in strain rate (Figure 7). This movement was not associated with a measured change in bulk sample pore-water pressure and was observed in all three samples, although more pronounced in experiments PWP 5 and PWP 3. The sliding phase developed at a similar normal effective stress (c.10 kPa) in each experiment, regardless of the rate of pore-pressure increase. The continued decrease in mean effective stress following this phase resulted in a progressive increase in horizontal strain which comprised of distinct periods of increasing strain rate punctuated by periods of reducing strain rate. This cyclic strain phase produced an exponential increase in strain rate with reducing mean effective stress (Figure 7).

The development of a short, near-instantaneous, sliding phase followed by repeating cyclic strain suggested that the shear zone mobilised and sheared at a critical mean effective stress without acceleration to runaway failure despite the continued reduction in mean effective stress. Instead, the strain rate continued to increase exponentially with pore-water pressure and therefore exhibited an asymptotic trend in 1/v-p' space (Figure 8). Despite some variability in behaviour between each experiment, the strong asymptotic trend observed in 1/v -p' space (Figures 8 A, B and C) demonstrated that each sample underwent ductile deformation after a critical mean effective stress was reached, regardless of the rate of pore-water pressure increase. Similar styles of behaviour have been observed in shallow terrestrial landslides (e.g. Allison and Brunsden, 1990) and have been shown to be controlled by localised pore fluid changes in laboratory experiments (e.g. Ng and Petley, 2009).

The PGP experiments showed broadly similar progressive strain development and shear-zone dilation in response to decreasing mean effective stress as observed in the PWP testing (Figure 6 A and B). However, whilst movement initiated at low horizontal strain rates ($< 0.05\ \mu S\ s^{-1}$) and high mean effective stress in both experiments (Figure 9 A), only PGP 12 developed the distinct sliding phase observed during the PWP experiments. This sliding phase occurred at a similar critical effective normal stress (c.10 kPa) to that in each of the PWP experiments indicating that pore fluid phase had negligible influence on the effective stress conditions required to mobilise the shear zone.

By comparison, PGP 30 experienced an exponential increase in strain rate to approximately 0.5 µS s^{-1} at a higher effective stress (15 kPa, Figure 9A). Following this, the strain rate remained constant whilst the mean effective stress continued to reduce. The peak strain rate was then reached at a lower effective stress (c.8 kPa) and resulted from a further exponential increase in strain rate. Whilst more variability was observed in PGP 30, similar maximum strain rates were observed in both PGP 30 and PWP 30 experiments, suggesting subtle differences in rheology may have impacted the testing. Similar episodic patterns of strain-rate development were observed in both gas experiments once the shear surface had mobilised, and an asymptotic trend in 1/v - p' space was observed in both PGP experiments (Figure 9 B).

The results indicated that shear-zone deformation occurred through ductile deformation at a critical mean effective stress regardless of the applied rate of pore pressure increase or the phase of the pore fluid. In addition, the distinct reduction in movement rates after initial shear surface mobilisation and the exponential increase in displacement rate observed across all experiments indicated that catastrophic failure did not develop. During most of the experiments, no relationship between reduction in strain rate and decreasing sample pore pressure was observed (e.g. Figure 10 A), however, a reduction in sample pore gas pressure was measured during experiment PGP30, which coincided with the development of peak horizontal and vertical strain rates (Figure 10 B). It was inferred from this that the rapid dilation of the shear zone acted to increase its permeability, which resulted in localised dissipation of pore water pressure, temporarily altering the stress state within the shear zone before pore pressure increased further. Slow episodic shear regulated by dilation provides a potential mechanism to explain the cyclic phases of increased landslide displacement rate observed in response to elevated pore-fluid pressures without the development of rapid shear failure.

5. DISCUSSION

Although a range of mechanisms have been suggested to explain various subaqueous mass-movements, including shear surface nucleation (e.g. Viesca and Rice, 2012); shear zone liquefaction and ductile extrusion (e.g. Bull et al., 2009; Sassa et al., 2012); and local lateral fluid flow (Dugan and Flemings, 2000; Fleming et al., 2002), very few mechanisms have been proposed to explain shallow subaqueous slope failures that arrest without long runout. Based on the experimental results illustrated herein, a conceptual model can be hypothesised to explain how shallow subaqueous slopes can progressively deform through episodic movement when pore-fluid pressures are elevated within a shear zone (Figure 11).

In the model, an increase in pore pressure generates localised dilation and strain within the landslide shear zone. As a consequence, very slow pre-failure deformation initiates whilst effective normal stress remains comparatively high in the slope (stage 2). Slow dilation increases the permeability of the shear zone allowing pore pressures to increase more rapidly which increases the landslide strain rate and drives further shear zone dilation (stage 3). This progressive increase in strain rate, and the associated inter-particle deformation, drives further increases in local pore-fluid pressure, within the narrow shear zone. This in turn induces a further increase in strain rate (stage 4). The feedback mechanism continues as pore water pressure increases to reach a critical mean effective stress when the shear surface rapidly slides and dilates (stage 5). This process rapidly changes the shear zone properties as the rate of permeability increase through dilation exceeds the rate of pore pressure increase within the narrow shear band. This leads to pore expansion and dissipation of the excess fluid pressure (stage 5), locally increasing the effective stress and reducing the shear strain rate. These processes prevent catastrophic acceleration (stage 6).

The process of coupling local pore-pressure increase and the development of high strain rate, checked by dilation and the broadening of the shear zone, can continue while external processes drive increasing pore-fluid pressure (stage 7a). Consequently, the landslide will continue to display ductile deformation behaviour, characterised by exponential increases in strain rate punctuated by episodic phases of decreased movement rates, never leading to catastrophic failure. Should the externally derived pore-fluid pressures reduce or pore fluid dissipate fully from the shear zone (Stage 7b) the slope movement will arrest and expulsion of pore fluid from the pores will result in re-compaction of the shear zone (stage 8).

Our study has focused specifically on the movement mechanisms in subaqueous slopes using a linear increase in pore-fluid pressure within a pre-defined shear zone. Other potential mechanisms hypothesised to influence landslide motion such as state-and-rate-variable friction affects (e.g. Helmsetter et al., 2004), complex perturbations in effective stress (e.g. Hangwerger et al., 2016) and shear-surface geometry (e.g. Aryal et al., 2015) have not been analysed. The coupling of shear deformation and shear-zone dilation observed in our experiments has been shown to promote steady landslide motion, particularly within clay-rich landslide shear zones (Iverson, 2005). Similar movement patterns are also observed in terrestrial landslides on shallow slopes, (e.g. Ng and Petley, 2009) and slowly deforming mudslides (e.g. Allison and Brunsden, 1990). In addition, similar behaviour has been used to describe ice flow dynamics (e.g. Damsgaard et al., 2016) and the pore fluid driven cyclic fault-valve model proposed for seismic slip (Sibson, 1992), indicating that this behaviour can be expected across a broad range of geological processes.

Despite the different physical properties of nitrogen gas and liquid water, similar patterns of behaviour were observed across all the experiments, demonstrating that either fluid can generate similar movement characteristics with increasing pore pressure. The results explain how unconstrained subaqueous landslides can episodically move downslope when pore-fluid pressures at the landslide shear zone are elevated by external factors such as the injection of water or gas from below.

The experiments presented herein provide credible support for the hypothesis that over-pressuring by free gas can result in episodic/slow movements required to produce submarine spreading failures observed in different parts of the world (e.g. Micallef et al., 2007; Mountjoy et al. 2009; Micallef et al. 2016). Cyclic changes in strain rate driven by a negative feedback mechanism associated with shear-zone dilation provides a credible mechanism through which a subaqueous landslide can accumulate large strain without catastrophic failure. This cyclic process, therefore, determines the long-term behaviour of subaqueous mass movement in shallow sedimentary sequences, and as similar materials commonly form submarine slopes, it is likely to be a widespread seafloor process.

CONCLUSION

Geomorphological evidence suggests that some shallow subaqueous slopes can accumulate substantial amounts of downslope deformation without transitioning to catastrophic failure, even though their downslope terminations are unconstrained (Mountjoy et al., 2009; Micallef et al., 2016). Novel laboratory experiments have been used to explore this behaviour by examining the response of such slope materials to states of low effective normal stress associated with high pore-fluid pressure induced by either gas or water injected from below. The strain behaviour observed in the experiments were found to be similar to the movement patterns measured in terrestrial landslides which deform along ductile shear zones. In such circumstances movement develops when pore water pressures are sufficiently elevated in the slope and movement rates increase exponentially with increasing pore pressure. Given that this response is dominated by the effective stress conditions operating within the shear zone, such behaviour can be expected in submarine slopes regardless of the pore fluid phase (gas or liquid). The behaviour we observed provides a mechanism through which subaqueous landslides may accumulate strain without undergoing catastrophic failure. This has important implications when assessing marine geohazards since these types of slope failure will not be tsunamigenic.

ACKNOWLEDGMENT

We thank Peter Barker, Stuart Read and Zane Bruce for laboratory support. Samples were provided by the National Institute of Water and Atmospheric Science (NIWA). Financial support has been provided through the GNS Science Strategic Development Fund, Marsden Fund Contract NIW1603, GNS and NIWA Strategic Science

Investment Funding and by the NERC/ESRC Increasing Resilience to Natural Hazards programme, grant NE/J01995X/1, and NERC/Newton Fund grant NE/N000315.

REFERENCES

Allison, R., and Brunsden, D., 1990, Some mudslide movement patterns: Earth Surface Processes and Landforms, v. 15, p. 297-311.

Anderson, S.A., and Sitar, N., 1995, Analysis of rainfall induced debris flows, Journal of Geotechnical Engineering. American Society of Civil Engineers. V, 121, P.544-552.

Aryal, A., Brooks, B., Reid, M.E., 2015, Landslide subsurface slip geometry inferred from 3-D surface displacement fields, Geophysical Research Letters, v. 42(5), p. 1411-1417.

Baeten, N. J., Laberg, J. S., Vanneste, M., Forsberg, C. F., Kvalstad, T. J., Forwick, M., Vorren, T. O., Haflidason, H., 2014, Origin of shallow submarine mass movements and their glide planes—Sedimentological and geotechnical analyses from the continental slope off northern Norway, Journal of Geophysical Research: Earth Surface v.119(11), p. 2335-2360.

Bull, S., Cartwright, J., Huuse, M., 2009, A subsurface evacuation model for submarine slope failure, Basin Research, v. 21, p. 433-443.

Brain, M.J., Rosser, N.J., Sutton, J., Snelling, K., Tunstall, N., and Petley, D.N., 2015, The effects of normal and shear stress wave phasing on coseismic landslide displacement: Journal of Geophysical Research: Earth Surface, v 120, p. 1009-1022.

Brand, E.W., 1981, Some thoughts on rain-induced slope failure, Proceedings 10th International Conference on Soil Mechanics and Foundation Engineering, San Francisco. Balkema. p. 2541-2578.

Carey, J.M., McSaveney, M.J., Lyndsell, B.M., Petley, D., 2016, Laboratory simulation of a slow landslide mechanism. In: S, Aversa et al. (eds.) Landslides and engineered slopes: experience, theory and practice: proceedings of the 12th International Symposium on Landslides. Boca Raton, Fla.: CRC Press, p. 557–564.

Carey, J.M., McSaveney, M.J., Petley, D.N., 2017, Dynamic liquefaction of shear zones in intact loess during simulated earthquake loading. Landslides, v. 14(3), p. 789-804.

Carey, J.M., Moore, R., Petley, D.N., 2015, Patterns of movement in the Ventnor landslide complex, Isle of Wight, southern England, Landslides, v. 12(6), p. 1107-1118.

Carey, J.M., Petley, D.N., 2014, Progressive shear-surface development in cohesive materials; implications for landslide behaviour, Engineering Geology, v. 177: p. 54-65.

Crutchley, G.J., Mountjoy, J.J., Pecher, I. A., Gorman, A., Henrys, S.A., 2016, Submarine slope instabilities coincident with shallow gas hydrate systems: Insights from New Zealand examples. In: G. Lamarche et al. (eds.), Submarine Mass

Movements and their Consequences, Advances in Natural and Technological Hazards Research 41, p. 401-409.

Dai, F.C., Lee, C.F., Wang, S.J. and Feng, Y.Y., 1999. Stress-strain behaviour of a loosely compacted volcanic-derived soil and its significance to rainfall-induced fill slope failures. Engineering Geology, v. 53, p. 359-370.

Damsgaard, A., Egholm, D. L., Beem, L. H., Tulaczyk, S., Larsen, N. K., Piotrowski, J. A., Siegfried, M. R., 2016, Ice flow dynamics forced by water pressure variations in subglacial granular beds, Geophysical Research Letters, v 43, p. 12-165 – 12-173.

Dugan, B., and Flemings. P.B., 2000, Overpressure and fluid flow in the New Jersey continental slope: Implications for slope failure and cold seeps: Science, v. 289, p. 288–291.

Elger, J., Berndt, C., Rupke, L., Krastel, S., Gross, F., Geissler, W.H., 2018, submarine slope failures due to pipe structure formation, Nature Communications, v. 9, 715.

Flemmings, P.B., Stump, B.B., Finkbeiner, T., Zoback, M., 2002, Flow focusing in overpressured sandstones: Theory, observations and applications, American Journal of Science, v. 302(10), p. 827-855.

Fukuzono, T. 1990. Recent studies on the time prediction of slope failures. Landslide News, v. 4, p. 9-12.

Hangwerger, A.l., Rempel, A.w., Skarbek, R.M., Roering, J.J., Hilley, G.E., 2016, Rate-weakening friction characterises both slow sliding and catastrophic failure of landslides, Proceeding of the National Academy of Sciences, v. 133(37), p. 10281-10286.

Helmsetter, A., Sornette, D., Grasso, J-R., Andersen, J., Gluzmann, S., Pisarenko, V., 2004, Slider block friction model for landslides: Application to Vaiont and La Clapiere landslides, Journal of Geophysical Research, 109(B2), 10.1029/2002JB002160.

Hungr, O., Leroueil, S., Picarelli, L., 2014, The Varnes classification of landslide types, an update, Landslides, v. 11, p. 167-194.

Iverson, R.M., 2005. Regulation of landslide motion by dilatancy and pore pressure feedback: Journal of Geophysical Research, v. 110, F02015.

Kilburn, C.J., and Petley, D.N., 2003. Forecasting giant, catastrophic slope collapse: lessons from Vajont Northern Italy: Geomorphology, v. 54, p. 21-32.

Kossel, E., Bigalke, N., Piñero, E., and Haeckel, M., 2013, The SUGAR Toolbox - A library of numerical algorithms and data for modelling of gas hydrate systems and marine environments, Bremerhaven, PANGAEA .

Krastel, S., Li, W., Urlaub, M., Georgioupoulou, A., Wynn, R. B., Schwenk, T., Stevenson, C., Feldens, P., 2018, Mass wasting along the NW African continental margin. In: D.G. Lintern et al., (eds). Subaqueous Mass Movements and Their Consequences: Assessing Geohazards, Environmental Implications and Economic Significance of Subaqueous Landslides. Geological Society, London, Special Publications, 477, https://doi.org/10.1144/SP477.36

Kuhlman, J., Orpin, A., Mountjoy, J.J., Crutchley, G., Henrys, S., Lunenburg, R., Huhn, K., 2018, GSL: Seismic and lithofacies characterization of a gravity core transect down the submarine Tuaheni Landslide Complex, northeastern New Zealand. In: (eds.) D. G. Lintern, D. C. Mosher, L. G. Moscardelli, P. T. Bobrowsky, C. Campbell, J. D. Chaytor, J. J. Clague, A. Georgiopoulou, P. Lajeunesse, A. Normandeau, D. J. W. Piper, M. Scherwath, C. Stacey and D. Turmel, SP477 Subaqueous Mass Movements and Their Consequences: Assessing Geohazards, Environmental Implications and Economic Significance of Subaqueous Landslides Geological Society of London Special Publications, 477. https://doi.org/10.1144/SP477.37

Locat, J., Lee, H.J., 2002, Submarine landslides: Advances and challenges, Canadian Geotechnical Journal, V. 36, p. 193-212.

Mansour, F.M., Morgenstern, N.R., and Martin, D.C., 2011, Expected damage from displacement of slow-moving slides: Landslides, v. 8, p. 117-131.

Massey, C.I., Petley, D.N., McSaveney, M.J., 2013, Patterns of movement in reactivated landslides. Engineering Geology, v. 159, p. 1-19.

Micallef, A., Masson, D.G., Berndt, C., Stow, D.A.V., 2007, Morphology and mechanics of submarine spreading: A case study from the Storegga Slide, Journal of Geophysical Research, 112:F03023.

Micallef, A., Mountjoy, J.J., Krastel, S., Crutchley, G., Koch, S., 2016, Shallow gas And the development of a weak layer in submarine spreading, Hikurangi Margin (New Zealand). In: G. Lamarche et al. (eds.), Submarine Mass Movements and their Consequences, Advances in Natural and Technological Hazards Research 41 ,p. 419-426.

Mountjoy, J.J., Pecher, I., Henrys, S., Crutchley, G., Barnes, P.M., and Plaza-Faverola, A., 2014, Shallow methane hydrate system controls ongoing, downslope sediment transport in a low-velocity active submarine landslide complex, Hikurangi margin, New Zealand: Geochemistry, Geophysics, Geosystems, v. 15, p. 4137-4156.

Mountjoy, J.J., McKean, J., Barnes, P.M., and Pettinga J.R., 2009, Terrestrial-style slow-moving earthflow kinematics in a submarine landslide complex: Marine Geology, v. 267, p.114-127.

Mountjoy, J. and Micallef, A. 2018. Submarine Landslides. In Micallef, Krastel and Savini (eds) Submarine Geomorphology Springer International Publishing. 556p

Ng, K-Y., and Petley, D.N., 2009, A process approach towards landslide risk management in Hong Kong, Quarterly Journal of Engineering Geology and Hydrogeology, v. 42, p. 1-13.

Orense, R., Farooq, K. and Towhata, I., 2004, Deformation behaviour of sandy slopes during rainwater infiltration. Soils and Foundations, v. 44(2), p. 15-30.

Petley, D.N., Bulmer, M.H. and Murphy, W. 2002. Patterns of movement in rotational and translational landslides. Geology, V.30, p.719-722

Petley, D.N., Higuchi, T., Petley, D.J., Bulmer, M.H. and Carey. J., 2005, The development of progressive landslide failure in cohesive materials: Geology, v. 33, p. 201-204.

Petley, D.N., Mantovani, F., Bulmer, M.H. & Zannoni, A. 2005c. The use of surface monitoring data for the interpretation of landslide movement patterns. Geomorphology, 66:133-147.

Petley, D.N. and Petley, D.J., 2006. On the initiation of large rockslides: perspectives from a new analysis of the Vaiont movement record. In: S.G Evans, G S Mugnozza, A Strom and R.L Hermanns (eds.), Landslides from Massive Rock Slope Failure. NATO Science Series IV: Earth and Environmental Sciences. Springer: Dordrecht. p. 77-84.

Riboulot, V., Cattaneo, A., Sultan, N., Garziglia, S., Ker, S., Imbert, P. and Voisset, M. 2013. Sea-level change and free gas occurrence influencing a submarine landslide and pockmark formation and distribution in deepwater Nigeria. Earth and Planetary Science Letters v. 375, p. 78-91.

Saito, M. (1965). Forecasting the time and occurrence of a slope failure. Proceedings of the 6th International Conference on Soil Mechanics and Foundation Engineering. 2. p. 537-541.

Sassa, K., He, B., Miyagi, T., Strasser, M., Konagai, K., Ostric, M., Setiawan, H., Takara, K., Nagai, O., Yamashiki, and Y., Tutumi, S., 2012, A hypothesis of the Senoumi submarine megaslide in Surga Bay in Japan – based on the undrained dynamic loading ring shear tests and computer simulation: Landslides, v. 9, p. 439-455.

Schulz, W., J. McKenna, J. Kibler and G. Biavati (2009). "Relations between hydrology and velocity of a continuously moving landslide—evidence of pore-pressure feedback regulating landslide motion?" Landslides, v. 6(3), p. 181-190.

Sibson, R. H., 1992, Implications of fault-valve behaviour for rupture nucleation and recurrence, Tectonophysics, v 211, p. 283-293.

Stigall, J., and Dugan, B., 2010, Overpressure and earthquake initiated slope failure in the Ursa region, northern Gulf of Mexico: Journal of Geophysical Research, v.115, B04101.

Talling, P.J., Wynn, R.B., Masson, D.G., Frenz, M., Cronin, B.T., Schiebel, R., Akhmetzhanov, A.M., Dallmeier-Tiessen, S., Benetti, S., Weaver, P.P.E., Georgiopoulou, A., Zühlsdorff C., Amy L.A., 2007, Onset of submarine debris flow deposition far from original giant landslide, Nature, v. 450(7169). p, 541-544.

Urlaub, M., Talling, P.J., Zervos, A., Masson, D., 2015, What causes large submarine landslides on low gradient (<2°) continental slopes with slow (~0.15 m/Kyr) sediment accumulation? Journal of Geophysical Research: solid Earth, v. 120, p. 6722-6739.

Viesca, R. C., and Rice, J.R., 2012, Nucleation of slip-weakening rupture instability in landslides by localized increase of pore pressure: Journal of Geophysical Research, v. 117, B03104.

Voight, B. 1988, A relation to describe rate dependent material failure. Science, v. 243, p. 200-203.

Zhu, J.-H., and Anderson, S.A., 1998, Determination of shear strength of Hawaiian residual soil subjected to rainfall-induced landslides. Geotechnique, v. 48(1), p. 73-82.

Wallace, L. M., and Beavan, J., 2010, Diverse slow slip behavior at the Hikurangi subduction 390 margin, New Zealand, Journal of Geophysical Research, v 115/ B007717

Wallace, L. M., Beavan, J., Bannister, S., and Williams, C., 2012, Simultaneous long-term and short-term slow slip events at the Hikurangi subduction margin, New Zealand: Implications for processes that control slow slip event occurrence, duration, and migration, Journal of Geophysical Research, v. 112/B009489.

FIGURE CAPTIONS

Figure 1. Study area, east of New Zealand's North Island. (A) 'Hillshade' plot of Tuaheni Basin bathymetry, showing the Tuaheni Landslide Complex (TLC) and a shallow subaqueous slope failure (Inset B) which both show evidence of limited displacement despite having unconstrained toes. Yellow dots = location of Sample Tan1404-10; yellow contours = metres below sea level adapted from Mountjoy et al. (2014). (B) Bathymetric map of shallow subaqueous slope failure draped over slope gradient map and showing key morphological features including arrested debris (ad) and evacuated debris (ed) after Micallef et al. (C) Seismic section across the subaqueous slope failure headscarp after Micallef et al. (2016).

Figure 2. The particle size distribution of samples EN1285 (Tan1404-01) and EN1287 (Tan1404-10) collected from the Tuaheni South section of the TLC.

Figure 3. Laboratory testing apparatus and procedures. (A) Schematic diagram of the Dynamic Back Pressure Shearbox apparatus. (B) Experimental procedure used for pore water pressure testing. (C) Experimental procedure used for pore gas pressure testing.

Figure 4. Testing parameters used during the specialist pore pressure reinflation testing. (A) Applied pore pressure (Back pressure) against mean effective stress. (B) Stress paths followed during the pore water pressure (PWP) and pore gas pressure (PGP) experiments in relation to the conventional failure envelope.

Figure 5. Residual strength envelopes constructed from conventional drained shear tests carried out on samples EN1285 and EN1287.

Figure 6. Change in horizontal and vertical strain measured during PWP and PGP experiments. (A) Horizontal strain against normal effective stress. (B) Vertical strain against normal effective stress.

Figure 7. Horizontal strain rate against normal effective stress illustrating three distinct movement phases measured during PWP experiments.

Figure 8. Analysis of movement styles observed during each PWP experiment using 1/ Horizontal strain rate (V) against normal effective stress (p'). (A) Asymptotic trend calculated during PWP 30 experiment. (B) Asymptotic trend calculated during PWP 12 experiment. (C) Asymptotic trend calculated during PWP 5 experiment.

Figure 9. Analysis of movement styles observed during each PGP experiment. (A) Horizontal strain rate against normal effective stress. (B) 1/ Horizontal strain rate (v) against normal effective stress (p'). (C) Asymptotic trend calculated during PGP 30 experiment. (D) Asymptotic trend calculated during PGP 12 experiment.

Figure 10. Comparison of behaviour observed during the PWP and PGP experiments. (A) Change in pore water pressure and strain rate against time measured during experiment PWP 30. (B) Change in pore gas pressure and horizontal strain rate against time measured during experiment PGP 30.

Figure 11. Conceptual model of the development of slow movement in the shallow subaqueous slopes driven by elevated pore-fluid pressure.

TABLE CAPTIONS

Table 1. Physical properties of the Tuaheni sediments

Table 2. Summary of conventional drained shear tests

Table 3. Summary of pore pressure reinflation tests

TABLE 1. PHYSICAL PROPERTIES OF THE TUAHENI SEDIMENTS

Sample Reference	EN1285 (Tan1404-02)		EN1287 (Tan1404-10)	
	Range	Average	Range	Average
Sampling depth (*mbsb)	0.32-0.49		2.23-2.40	
Moisture content (%)	77.0-80.0	78.5	70.0-72.0	70.5
Void ratio	3.11-3.17	3.14	2.00-2.18	2.06
Dry density	0.65-0.66	0.65	0.85-0.90	0.88
Atterberg limits:				
Plastic limit (%)	75		76	
Liquid limit (%)	35		32	
Plasticity index (%)	40		44	
Particle size distribution:				
Clay (%)	5.50		4.18	
Silt (%)	88.18		88.48	
Sand (%)	6.32		7.33	

*mbsb = meters below sea bed

TABLE 2. SUMMARY OF CONVENTIONAL DRAINED SHEAR TESTS

Sample number	Sample depth (mbsl)	Initial water content w_n (%)	Void Ratio	Dry density ρ_d (t/m^3)	Normal stress (kPa)	Shear stress (kPa)	
						Peak	Residual
EN1285a	0.40–0.44	78	3.14	0.65	32	27	27
EN1285c	0.36–0.40	77	3.11	0.66	76	59	59
EN1285d	0.32–0.36	79	3.17	0.65	10	11	11
EN1287a	2.31–2.35	70	2.02	0.89	32	31	31
EN1287c	2.27–2.31	72	2.18	0.85	10	12	12
EN1287e	2.23–2.27	70	2.00	0.90	76	66	66

TABLE 3. SUMMARY OF PORE PRESUSRE REINLFATION TESTS

Test Reference	Sample Number	Normal effective stress (kPa)	Initial shear strength (kPa)	Post failure shear stress/ Percentage of initial shear strength (kPa) / (%)	Pore fluid increase rate (kPa/ hr)	Pore fluid
PWP 5	EN1287i*	32*	22	15 (68%)	5	water
PWP 12			20	15 (75%)	12	water
PWP 30	EN1287p	32	20	13 (65%)	30	water
PGP 12	EN1287q	32	20	13 (65%)	12	nitrogen
PGP30	EN1287k	32	19	13 (68%)	30	nitrogen

*Test PWP 5 and PWP 12 conducted on the same sample

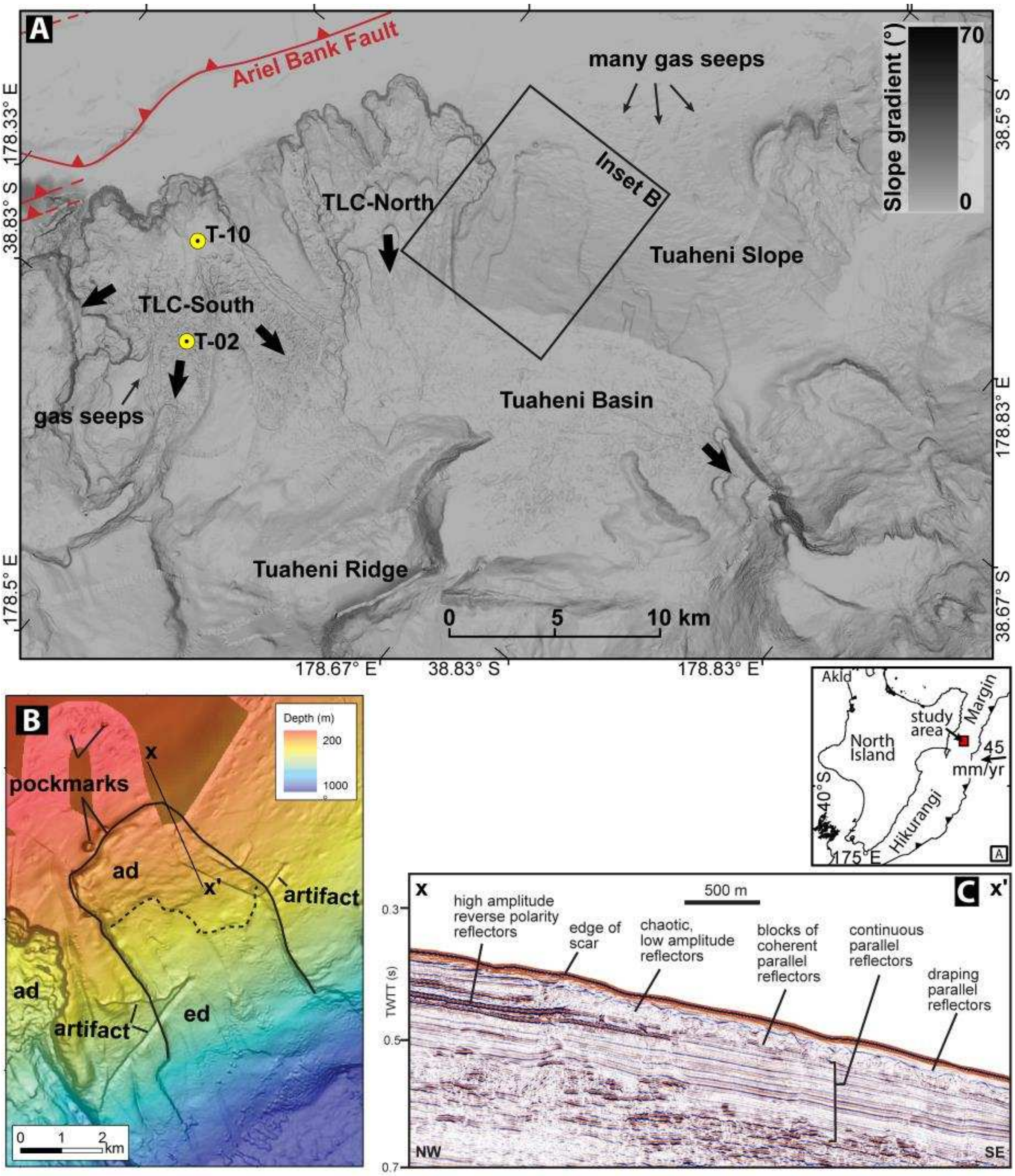

Figure 1. Study area, east of New Zealand's North Island. (A) 'Hillshade' plot of Tuaheni Basin bathymetry, showing the Tuaheni Landslide Complex (TLC) and a shallow subaqueous slope failure (Inset B) which both show evidence of limited displacement despite having unconstrained toes. Yellow dots = location of Sample Tan1404-10; yellow contours = metres below sea level adapted from Mountjoy et al. (2014). (B) Bathymetric map of shallow subaqueous slope failure draped over slope gradient map and showing key morphological features including arrested debris (ad) and evacuated debris (ed) after Micallef et al. (C) Seismic section across the subaqueous slope failure headscarp after Micallef et al. (2016).

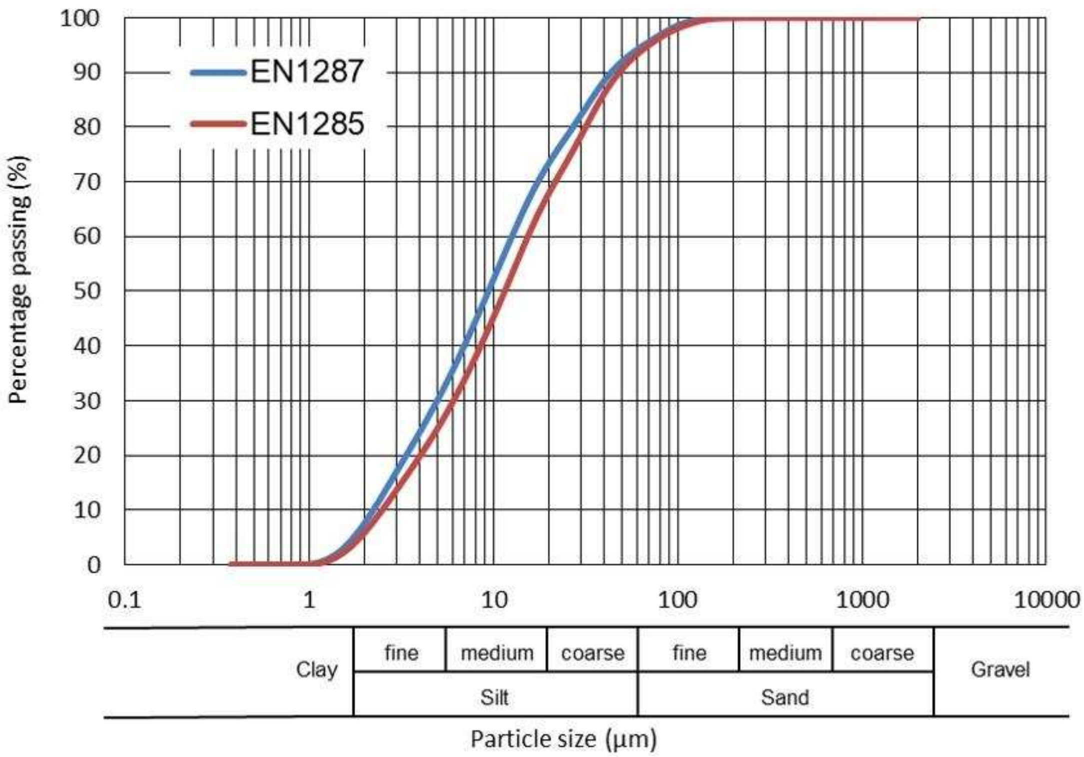

Figure 2. The particle size distribution of samples EN1285 (Tan1404-01) and EN1287 (Tan1404-10) collected from the Tuaheni South section of the TLC.

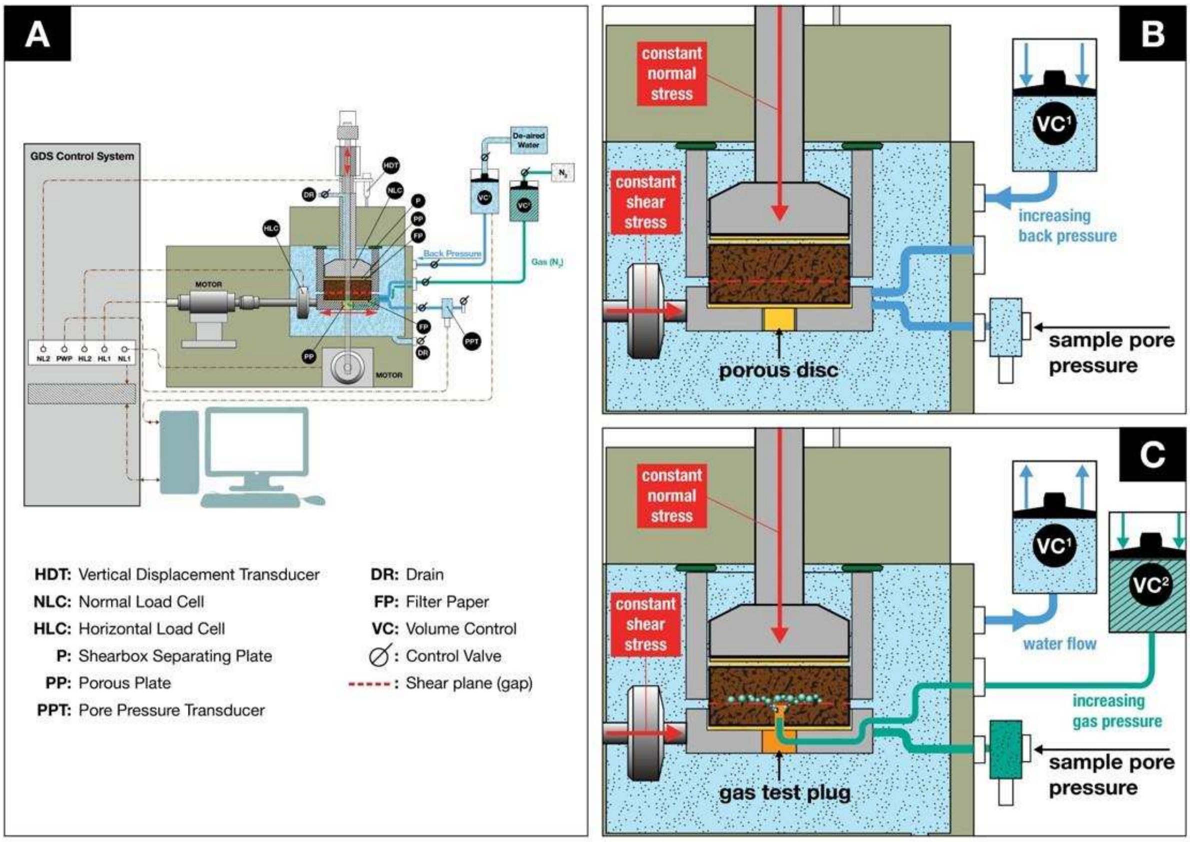

Figure 3. Laboratory testing apparatus and procedures. (A) Schematic diagram of the Dynamic Back Pressure Shearbox apparatus. (B) Experimental procedure used for pore water pressure testing. (C) Experimental procedure used for pore gas pressure testing.

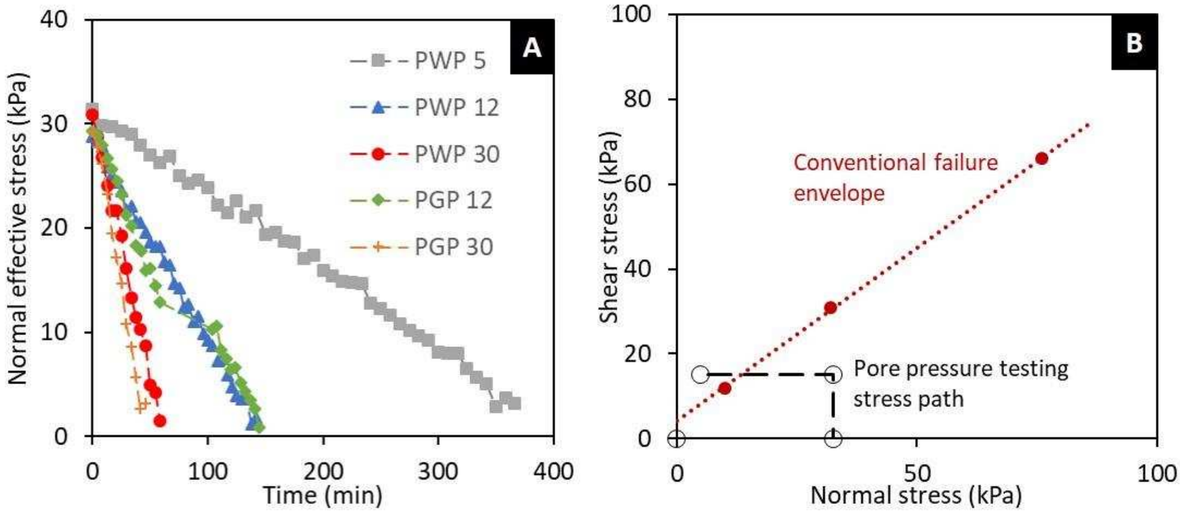

Figure 4. Testing parameters used during the specialist pore pressure reinflation testing. (A) Applied pore pressure (Back pressure) against mean effective stress. (B) Stress paths followed during the pore water pressure (PWP) and pore gas pressure (PGP) experiments in relation to the conventional failure envelope.

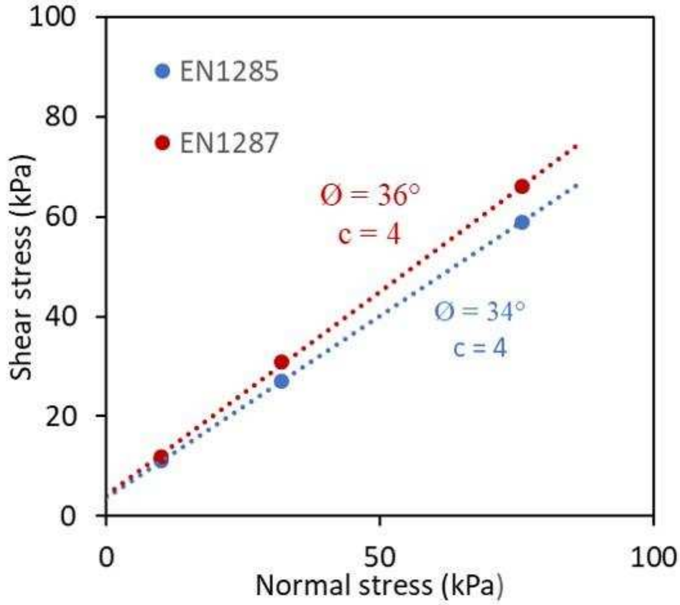

Figure 5. Residual strength envelopes constructed from conventional drained shear tests carried out on samples EN1285 and EN1287.

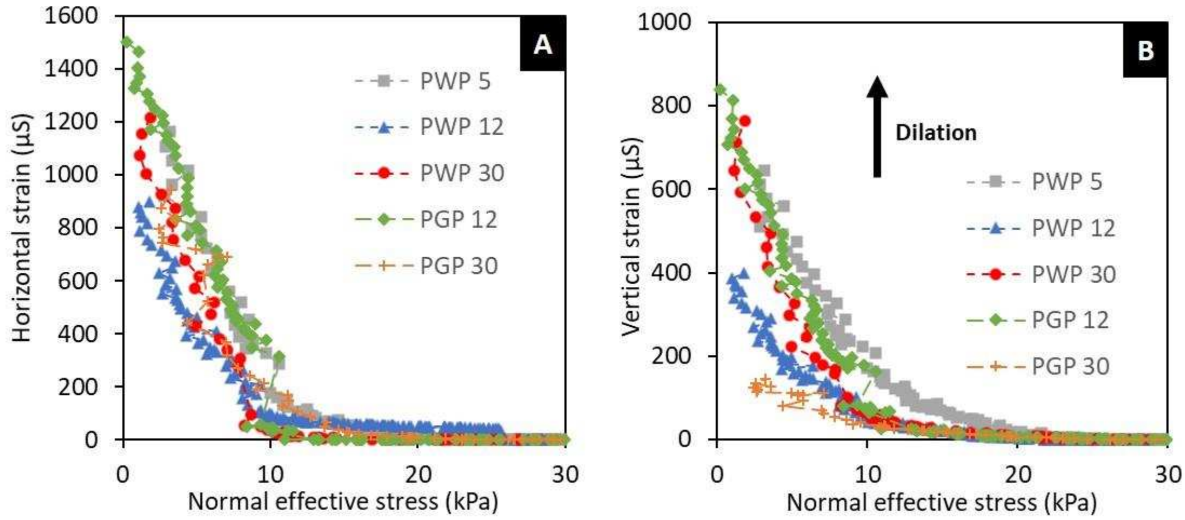

Figure 6. Change in horizontal and vertical strain measured during PWP and PGP experiments. (A) Horizontal strain against normal effective stress. (B) Vertical strain against normal effective stress.

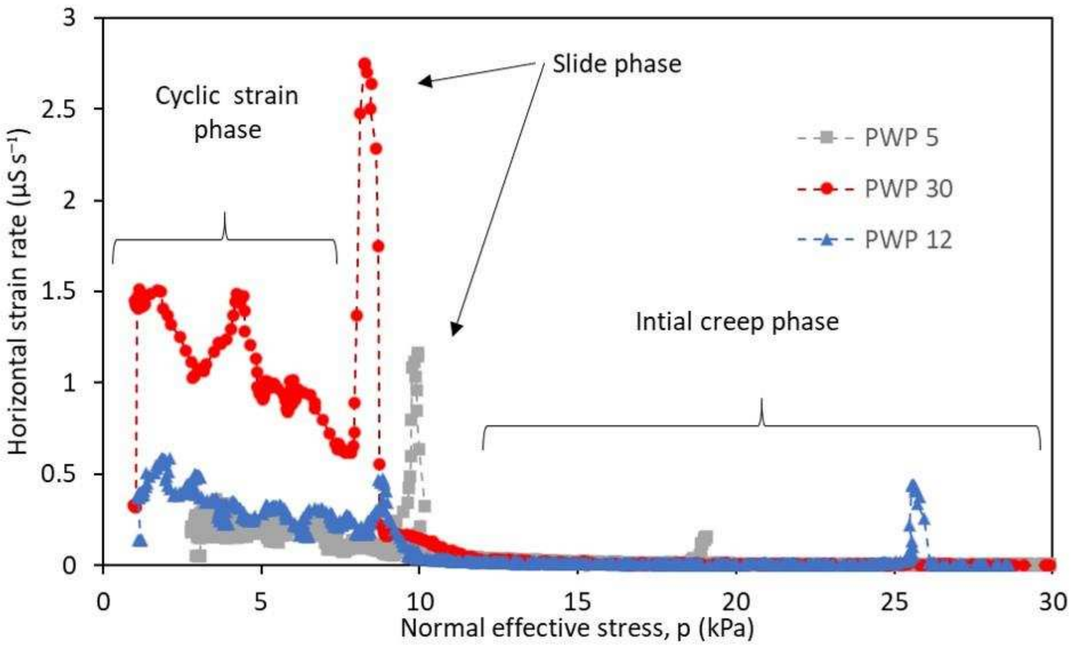

Figure 7. Horizontal strain rate against normal effective stress illustrating three distinct movement phases measured during PWP experiments.

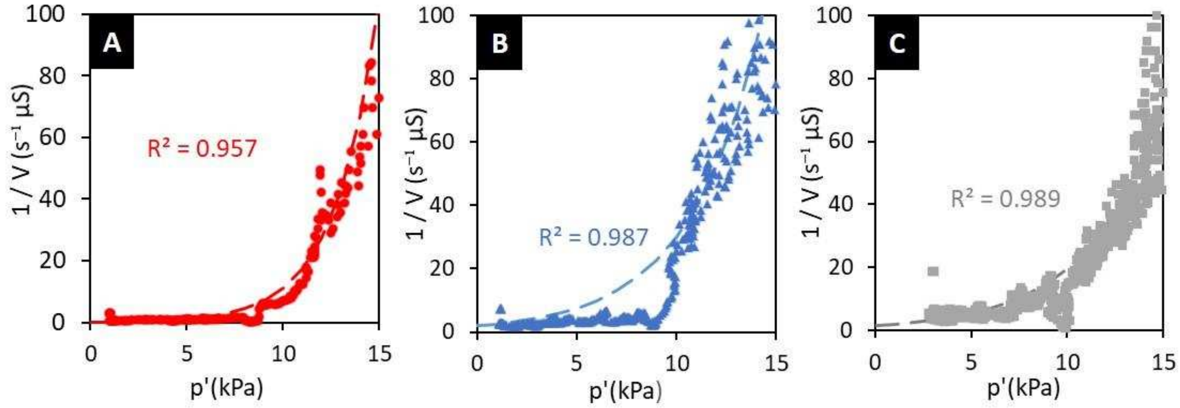

Figure 8. Analysis of movement styles observed during each PWP experiment using 1/ Horizontal strain rate (V) against normal effective stress (p’). (A) Asymptotic trend calculated during PWP 30 experiment. (B) Asymptotic trend calculated during PWP 12 experiment. (C) Asymptotic trend calculated during PWP 5 experiment.

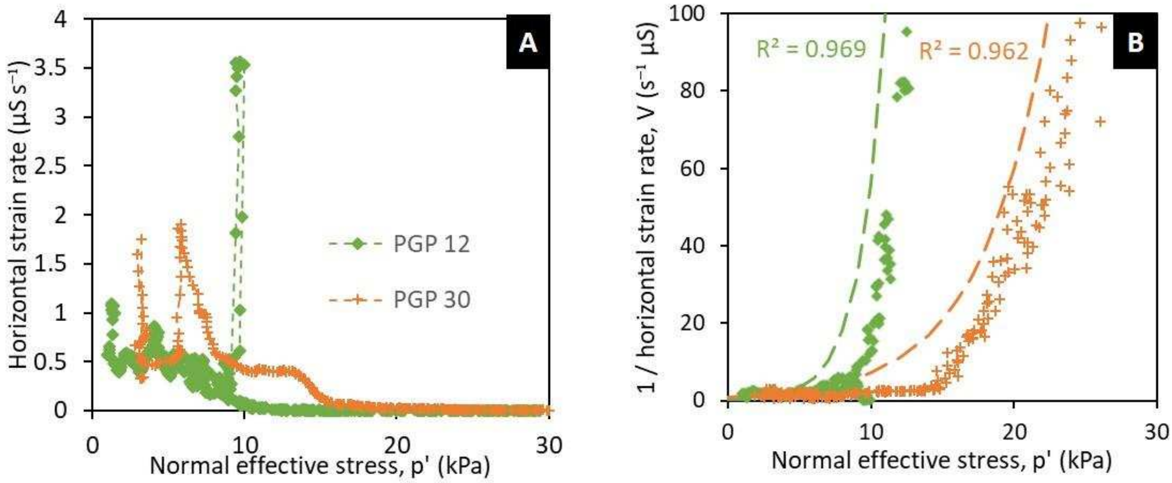

Figure 9. Analysis of movement styles observed during each PGP experiment. (A) Horizontal strain rate against normal effective stress. (B) 1/ Horizontal strain rate (v) against normal effective stress (p'). (C) Asymptotic trend calculated during PGP 30 experiment. (D) Asymptotic trend calculated during PGP 12 experiment.

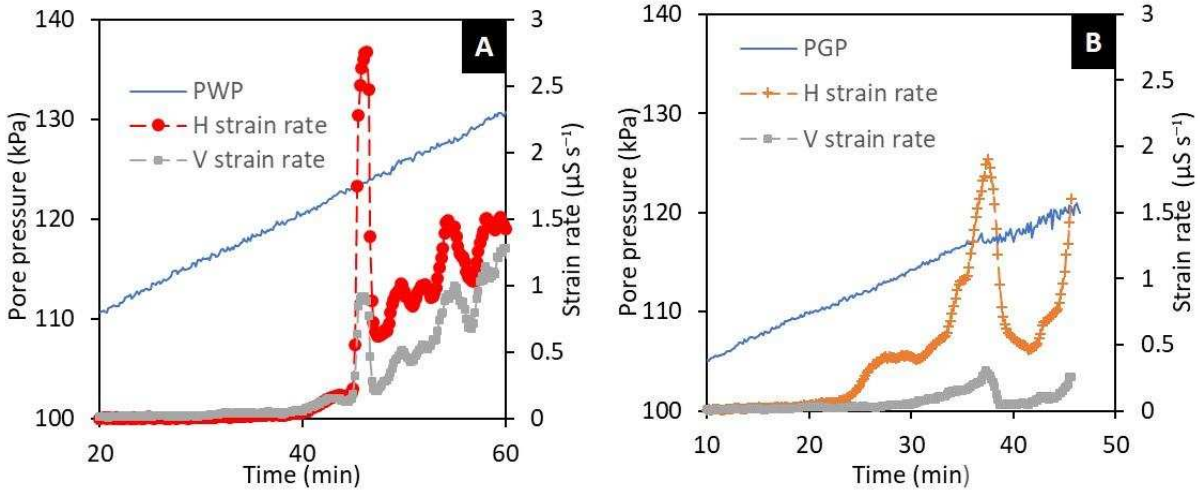

Figure 10. Comparison of behaviour observed during the PWP and PGP experiments. (A) Change in pore water pressure and strain rate against time measured during experiment PWP 30. (B) Change in pore gas pressure and horizontal strain rate against time measured during experiment PGP 30.

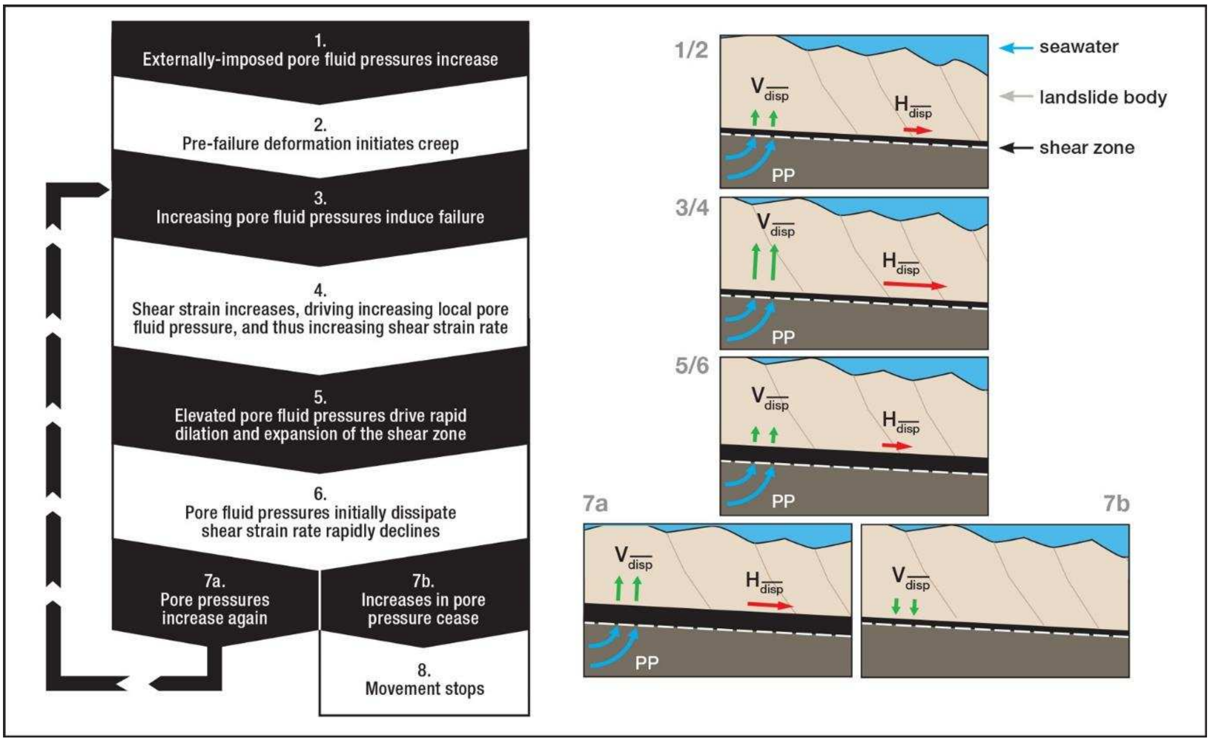

Figure 11. Conceptual model of the development of slow movement in the shallow subaqueous slopes driven by elevated pore-fluid pressure.